Polymer Journal (2019) 51:761–770
https://doi.org/10.1038/s41428-019-0189-0

ORIGINAL ARTICLE

Hydrophobic poly(3,4-ethylenedioxythiophene) particles synthesized by aqueous oxidative coupling polymerization and their use as near-infrared-responsive liquid marble stabilizer

Natsuko Shimogama[1] · Makoto Uda[1] · Keigo Oyama[1] · Haruka Hanochi[2] · Tomoyasu Hirai[1,3] · Yoshinobu Nakamura[1,3] · Syuji Fujii[1,3]

Received: 14 February 2019 / Accepted: 12 March 2019 / Published online: 2 April 2019

Abstract

The aqueous oxidative coupling polymerization of 3,4-ethylenedioxythiophene was conducted in the presence of heptadecafluorooctane sulfonic acid, which was used as a perfluoroalkyl dopant to synthesize hydrophobic poly(3,4-ethylenedioxythiophene) particles. The poly(3,4-ethylenedioxythiophene) particles were characterized in terms of their size, morphology, surface and bulk chemical compositions, conductivity, hydrophilic–hydrophobic balance and (photo)thermal properties. The electron microscopy studies confirmed that poly(3,4-ethylenedioxythiophene) consisted of aggregates of primary atypical particles of a submicrometer size. X-ray photoelectron spectroscopy and the contact angle measurement indicated that the perfluoroalkyl dopants were present on the surface of the poly(3,4-ethylenedioxythiophene) particles, which caused them to have a hydrophobic character. The electrical conductivity of the pressed pellet was 15.5 S cm^{-1}, which was one order of magnitude higher than that of the poly(3,4-ethylenedioxythiophene) that was synthesized in the absence of the perfluoroalkyl dopant. The dried poly(3,4-ethylenedioxythiophene) particles could be used as a near-infrared-responsive liquid marble stabilizer exhibiting light-to-heat conversion properties. The movement of the poly(3,4-ethylenedioxythiophene) particle-coated liquid marbles on a planar water surface was driven by near-infrared laser-induced Marangoni propulsion. The inner liquid could be released by the disruption of the liquid marbles via an application of an external stimulus.

Introduction

Compared to polypyrrole (PPy) and polyaniline (PANI), poly(3,4-ethylenedioxythiophene) (PEDOT) is an attractive conjugated polymer that has gained much interest due to its improved environmental stability under ambient conditions and at raised temperatures [1–4]. PEDOT has 3,4-disubstituted thiophene rings, which block the sites necessary for carbonyl formation, and therefore, overoxidation, as well as cross-linking that occurs during polymerization, can be suppressed. In addition, due to its low coloration, PEDOT has applications for use as an antistatic material and a component in electrical and electronic devices [1–4]. Recently, it was confirmed that PEDOT has a high optical absorbance in the near-infrared (NIR) region, which leads to an excellent capability for light-to-heat photothermal conversion [5].

Liquid marbles (LMs) are nonstick liquid droplets with sizes between a millimeter and a centimeter that are wrapped with hydrophobic solid particles in the gas phase [6–9]. LMs can be easily fabricated by rolling the droplets in particle powders in air, and the LMs are able to move easily

These authors contributed equally: Natsuko Shimogama, Makoto Uda

Supplementary information The online version of this article (https://doi.org/10.1038/s41428-019-0189-0) contains supplementary material, which is available to authorized users.

✉ Syuji Fujii
syuji.fujii@oit.ac.jp

[1] Department of Applied Chemistry, Faculty of Engineering, Osaka Institute of Technology, 5-16-1 Omiya, Asahi-ku, Osaka 535-8585, Japan

[2] Division of Applied Chemistry, Graduate School of Engineering, Osaka Institute of Technology, 5-16-1, Omiya, Asahi-ku, Osaka 535-8585, Japan

[3] Nanomaterials Microdevices Research Center, Osaka Institute of Technology, 5-16-1, Omiya, Asahi-ku, Osaka 535-8585, Japan

on both solid and liquid surfaces due to their nonwetting character. Recently, stimuli-responsive LMs, whose shape, structure, stability and movement can be controlled by external stimuli, such as pH, light, temperature, ultrasonic waves and electric and magnetic fields, are receiving increased attention [9]. Due to their stimuli-responsive functions, potential applications of LMs have been proposed, including sensors [10–12], miniature reactors [13–17], microfluidics [18], pressure-sensitive adhesives [19], cosmetics [20], and material delivery carriers [21–26].

Fujii and coworkers recently synthesized hydrophobic PPy and PANI particles by aqueous oxidative coupling polymerization using perfluoroalkyl dopants by a one-pot and one-step method. In addition, it was confirmed that the dried particles work as an effective LM stabilizer exhibiting light-to-heat conversion properties [21–24]. Furthermore, it was demonstrated that the movement of LMs on a planar water surface can be induced by laser light irradiation-based Marangoni propulsion [21–24]; anisotropic heat distribution was generated around LMs that were floating on a planar air–water surface by the local NIR laser irradiation of LMs coated with PPy and PANI particle shells.

In this study, we extend our previous studies on PPy and PANI to PEDOT and report the facile synthesis of hydrophobic PEDOT particles by aqueous oxidative coupling polymerization using a perfluoroalkyl dopant (Fig. 1a). The size, size distribution, morphology, surface and bulk chemical compositions, density, hydrophilic–hydrophobic balance, conductivity and (photo)thermal properties of the PEDOT particles were investigated in detail. An aim of this study is the application of the aqueous oxidative coupling polymerization used for the syntheses of hydrophobic PPy and PANI to PEDOT, and PEDOT produced by this method was compared to the PEDOT synthesized without the perfluoroalkyl dopant. Furthermore, the synthesized hydrophobic PEDOT particles were used as an LM stabilizer exhibiting light-to-heat conversion properties (Fig. 1b). The movement of the LMs on the planar air–water interface was driven by near-infrared light-induced Marangoni flow, and analyses of the velocity, acceleration, generated force and velocity decay time of the movement were conducted. Furthermore, the stimulus-response disruption of the LM was also demonstrated.

Materials and methods

Synthesis of hydrophobic PEDOT materials

Aqueous oxidative coupling polymerizations were used to synthesize the PEDOT materials as follows (Table S1). Deionized water (8.0 g) was added to a mixture of 3,4-ethylenedioxythiophene (EDOT, Sigma-Aldrich, St Louis, MO, USA: 0.1 g, 7.03×10^{-4} mol) and heptadecafluorooctane sulfonic acid (C8F, Sigma-Aldrich, St Louis, MO, USA: 0–0.297 g) in a 13 mL screw-capped bottle, and the system was sonicated for 30 min using a ultrasonic bath (M2800-J, Branson Ultrasonics, Emerson Japan, Tokyo, Japan) to form white turbid EDOT-in-water emulsions. A ferric chloride oxidant ($FeCl_3 \cdot 6H_2O$, Sigma-Aldrich, St Louis, MO, USA: 0–0.297 g: 0.887 g, 3.28×10^{-3} mol) was dissolved in 3.0 g of deionized water and then added to the emulsions consisting of EDOT and C8F. The polymerizations were conducted at 70 °C for 24 h with magnetic stirring. Here, C8F works as both a dopant to neutralize the cation-charged PEDOT backbone and a hydrophobizer. To investigate the effects of the C8F concentration on the yield of the resulting PEDOT materials, the polymerizations were conducted at various C8F concentrations (EDOT/C8F molar ratios of 3/0, 3/0.01, 3/0.05, 3/0.1, 3/0.5, 3/1.0, 3/1.5, 3/2.0 and 3/2.5). The PEDOT materials were subsequently purified by repeated centrifugation-redispersion cycles

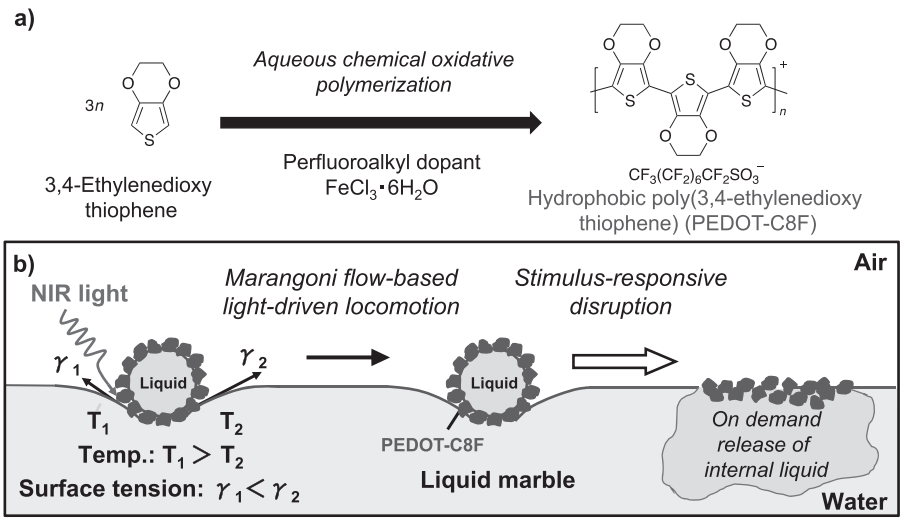

Fig. 1 **a** Synthesis of heptadecafluorooctane sulfonic acid-doped hydrophobic poly (3,4-ethylenedioxythiophene) (PEDOT-C8F) by aqueous oxidative coupling polymerization. **b** Schematic diagram illustrating movement of a liquid marble (LM) on a planar air–water interface driven by near-infrared (NIR) light irradiation-induced Marangoni flow and stimulus-responsive disruption of the LM followed by the release of its inner liquid

(where successive supernatants were replaced with deionized water).

Characterization of PEDOT materials

The volume mean diameter (D_v) of the PEDOT materials was analyzed using a particle size analyzer (Malvern Mastersizer 2000, Malvern, UK) and Malvern software. The morphology of the PEDOT materials was studied using an optical microscope (Motic BA200, Shimadzu, Kyoto, Japan) in the wet-state and a scanning electron microscope (SEM) (VE-8800 instrument, Keyence, Osaka, Japan) in the dried-state. The perfluoroalkyl dopant-loading of the PEDOT particles was determined by elemental microanalyses; fluorine content microanalysis (NAC Techno-service Co., Ltd., Chiba, Japan) and CHN elemental microanalyses (CHN-Corder MT-5, Yanaco, Tokyo, Japan) were conducted. The surface chemistry of the PEDOT materials was characterized by X-ray photoelectron spectroscopy (XPS) using an AXIS Ultra spectrometer equipped with a monochromated AlKα X-ray gun. The static contact angles of the liquid droplets (5 μL) were measured on pressed pellets 30 s after deposition using an SImage02 apparatus (Excimer Inc., Kanagawa, Japan). The densities of the dried PEDOT materials were determined using a helium pycnometer (AccuPyc II 1340 apparatus, Micromeritics, GA, USA). Thermogravimetric analysis (TGA) was conducted using a TGA instrument (Pyris 1, Perkin-Elmer Inc., MA, USA). The electrical conductivity of the dried PEDOT pressed pellets was determined using a resistivity meter (Loresta-GP MCP-T610, Mitsubishi Chemical Co., Tokyo, Japan) by the conventional four-point-probe method. Thermographic analysis was conducted using an 890-2 thermal imager (Testo, Lenzkirch, Germany). Refer to the Supplementary Information for details on the characterization methods.

Formation of LMs

The water droplets (15 μL) were rolled for 30 s on dried hydrophobic PEDOT powder that was slightly compacted on glass Petri dishes. The LMs were stabilized by PEDOT particles that were adsorbed at the air–water interface of the droplets.

Near-infrared light-controlled movement

A NIR laser (808 nm; output power, ~ 200 mW; spot diameter, $1 \times 5\ mm^2$), which was purchased from Changchun New Industries, Optoelectronics Technology, Co. Ltd. (Changchun, China), irradiated the LMs placed on the planar air–water surface, and the laser was aimed at the three-phase contact line. The movement was imaged using a digital camera (Ricoh G700SE; 5.0×optical zoom lens, Ricoh, Tokyo, Japan) and a digital video camera (Sony Handycam HDR-CX270 V; 30×optical zoom lens, Sony Co., Tokyo, Japan). The movement analyses were conducted using commercial software (Keyence VW-9000 MotionAnalyzer, Keyence, Osaka, Japan). For details on the analytical method, refer to the Supplementary Information.

Results and discussion

Synthesis and characterization of hydrophobic PEDOT materials

The oxidative coupling polymerization of EDOT proceeds with a reaction stoichiometry of 2.33 moles of electrons per mole of the monomer [1]. The $FeCl_3$/EDOT molar ratio was adjusted to 4.67 to obtain enough conversions of EDOT. It was reported that a higher concentration of $FeCl_3$ compared to the stoichiometric amount led to the production of PEDOT with enough conversions [1]. After the addition of the $FeCl_3$ oxidant to the aqueous solutions containing the C8F and EDOT monomer, the reaction solution turned green and then dark blue, which clearly indicates the production of PEDOT by polymerization. The products were purified by centrifugal washing (15 times) using deionized water and freeze dried. The yields of the PEDOT materials, which were gravimetrically determined, were below 27% for EDOT/C8F molar ratios at and below 3/0.5 and at the highest value of 70% for an EDOT/C8F molar ratio of 3/1 (Table S1). Considering that the yield of the PEDOT material synthesized with a molar ratio of 3/1 was higher than that of the material synthesized at and below 3/0.5, C8F promotes the polymerization of the EDOT monomer. The higher yield could have been due to the polymerization in the micelles/droplets formed by C8F and the effective doping of PEDOT with C8F. For EDOT/C8F molar ratios at and above 3/1.5, the yield gradually decreased with an increase in the C8F concentration (Table S1). This result could have occurred due to the removal of small PEDOT-C8F particles and PEDOT oligomers, which did not sediment during centrifugal purification. Hereafter, the PEDOT-C8F material synthesized with an EDOT/C8F molar ratio of 3/1 was characterized in comparison to the PEDOT synthesized in the absence of C8F (PEDOT-Cl), and the PEDOT-C8F material was used as an LM stabilizer because of its highest yield.

The laser diffraction particle size distribution analysis indicated the production of the PEDOT-C8F material with a volume-average diameter (D_v) of 21 ± 21 μm (Fig. 2a), which agreed with the results obtained by optical microscopy (Fig. 2b). Due to the interaction between the cationic

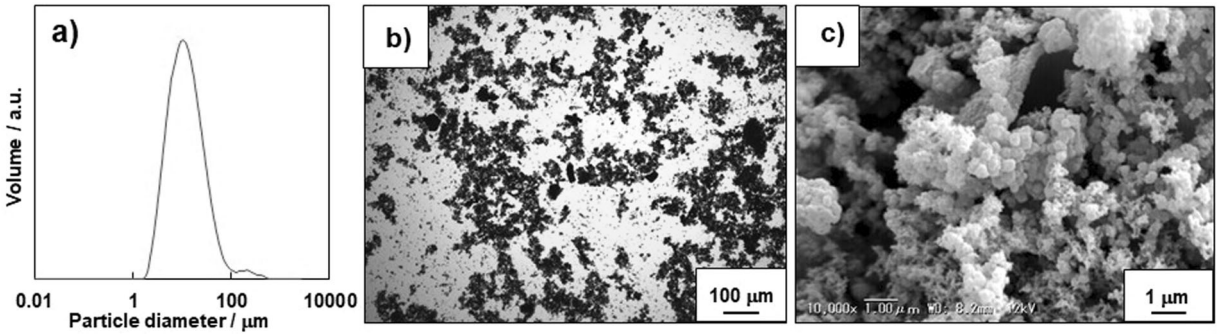

Fig. 2 **a** Particle size distribution curve measured by laser diffraction particle size analysis, **b** optical micrograph and **c** SEM image of PEDOT-C8F particles synthesized by aqueous oxidative coupling polymerization

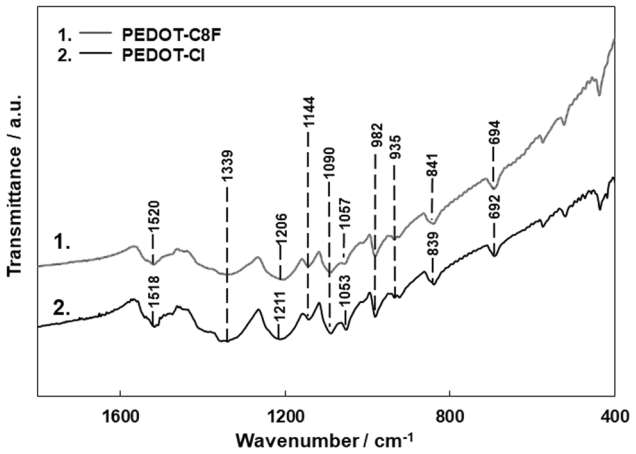

Fig. 3 FT-IR spectra of PEDOT materials: 1) PEDOT-C8F; 2) PEDOT-Cl

PEDOT and the anionic sulfonic acid groups of the perfluoroalkyl dopants, the perfluoroalkyl moiety was expected to protrude into the aqueous medium, which could lead to the flocculation of PEDOT nuclei rather than the formation of colloidally stable particles. The PEDOT-C8F material was a deep purple-colored powder after drying under vacuum. The SEM observations confirmed that atypical PEDOT primary particles with a submicrometer size were interconnected and formed aggregates (Fig. 2c).

The chemical compositions of the PEDOT materials were characterized by the FT-IR studies (Fig. 3). In the PEDOT-Cl spectrum, the characteristic peaks at ~1520 cm^{-1} and 1340 cm^{-1} were assigned to the asymmetric stretching mode of C = C and the inter-ring stretching mode of C-C, respectively. The peaks at ~1211 cm^{-1}, 1144 cm^{-1}, 1090 cm^{-1} and 1053 cm^{-1} were assigned to the C-O-C bending vibration in the ethylenedioxy group, and the peaks at 982 cm^{-1}, 935 cm^{-1}, 839 cm^{-1} and 692 cm^{-1} were characteristic of the stretching vibrations of the C-S-C bond in the thiophene ring [27]. In the case of PEDOT-C8F, a similar spectrum to that of PEDOT-Cl was obtained. The C8F spectrum showed a characteristic peak band at ~1200–1300 cm^{-1} [28], which corresponded to the vibration of the CF_3 and CF_2 groups, and the peaks caused by PEDOT-Cl and C8F overlapped with one another.

The mass percent of the C8F dopant loading was calculated to be 32 wt% by comparing its fluorine content with that of C8F. The theoretical mass percent of the dopant loading, which was determined assuming there was one dopant per three EDOT units in PEDOT [1], was calculated to be 54 wt%. The experimental dopant loading was lower compared to theory, and the lower C8F dopant loading could be explained by the coexistence of the chloride ion dopant originating from $FeCl_3$. Elemental microanalysis studies of Cl and S offer useful information on the doping level with the chloride ions. The Cl/S atomic ratio was 0.25 for PEDOT-Cl, indicating the presence of one chloride ion per four EDOT units, and decreased to 0.02 for PEDOT-C8F. This result provides strong evidence that C8F acts as a more efficient dopant compared to the chloride ions, as in the cases of PPy [23] and PANI [24].

The densities of the dried PEDOT-C8F and PEDOT-Cl materials were 1.73 ± 0.01 g cm^{-3} and 1.64 ± 0.01 g cm^{-3}, respectively, as shown in Table 1. The density of the C8F dopant was 2.731 g cm^{-3}, which is larger than that of PEDOT-Cl. These results confirmed that C8F, which has a higher density than the Cl^- anion, was incorporated into the PEDOT material as a dopant; this agreed with the elemental microanalysis results, as shown in Table 1.

The TGA performed in an N_2 atmosphere confirmed the occurrence of a gradual weight loss of the PEDOT-Cl material, and a final weight loss was determined to be ~75% at 1000 °C (Fig. 4). The PEDOT component did not decompose completely under an N_2 atmosphere, but it could be transformed into carbon-rich materials, as in the case of PPy [29, 30] and PANI [31, 32]. The PEDOT-C8F material exhibited an overall weight loss of 80% (Fig. 4). This larger weight loss could be due to the elimination of the C8F dopant from the PEDOT-C8F material at approximately 300–400 °C. A rapid weight loss was observed for pure C8F at approximately 190 °C [24], which was lower than the

Table 1 Elemental microanalyses, C8F loading, density, conductivity and 5 wt% weight loss temperature data for PEDOT-C8F and PEDOT-Cl materials

Samples	Cl (%)	S (%)	F (%)	Cl/S	C8F loading (%)	Density (g cm^{-3})	Conductivity (S cm^{-1})	5 wt% weight loss temperature (°C)
PEDOT-C8F	0.01	0.49	0.95	0.02	32	1.733 ± 0.010	15.54 ± 0.02	292
PEDOT-Cl	0.15	0.59	–	0.25	–	1.636 ± 0.006	3.82 ± 0.03	81

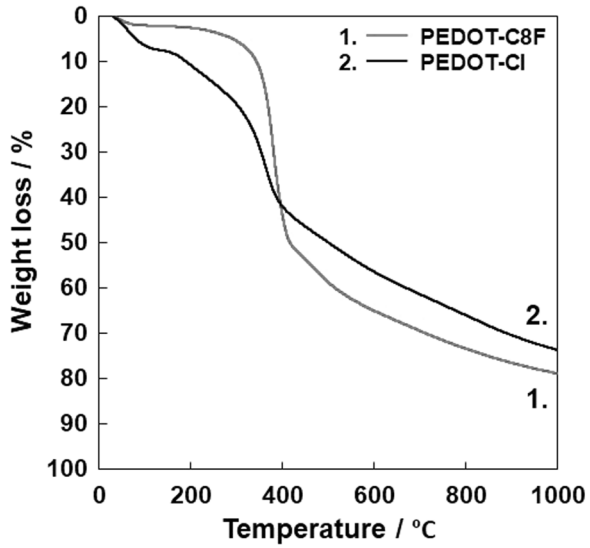

Fig. 4 TGA profiles of PEDOT materials: 1) PEDOT-C8F; 2) PEDOT-Cl

weight loss temperature detected in the PEDOT-C8F system. The higher weight loss temperature could have been due to the electrostatic interaction between the cationic PEDOT and the anionic C8F. The weight loss observed below 100 °C could have been due to the evaporation of the water molecules adsorbed by the PEDOT materials. A larger weight loss was detected for PEDOT-Cl compared to PEDOT-C8F, which could have been due to the more hydrophilic PEDOT-Cl surfaces that could adsorb a larger amount of water molecules (see below).

The existence of C8F on the surface of the PEDOT-C8F particles was verified by the XPS and water contact angle studies. The XPS survey spectra for the PEDOT-C8F and PEDOT-Cl materials are shown in Fig. 5a. In both materials, signals were observed for C, O and S. In the spectrum of the PEDOT-C8F particles, a signal assigned to F was clearly observed in addition to the signals assigned to C, O and S. The signal assigned to F originated from the C8F dopant on the PEDOT-C8F particle surfaces and indicated that C8F electrostatically interacted with the cationic PEDOT chains as a dopant. The nature of the interaction between the surface of PEDOT and the adsorbed C8F dopant was investigated using the high-resolution XPS spectra (Fig. 5b–d and Table 2). In the S p2 high-resolution spectrum of PEDOT-C8F, a shoulder peak was observed at 167 eV, which was assigned to S of the C8F dopant [23, 24], in addition to a peak at 163 eV, which originated from PEDOT. The surface Cl/S atomic ratio determined for PEDOT-C8F was negligible, while that of PEDOT-Cl was 0.47. The measured fluorine atomic percentage in PEDOT-C8F was over 30%. The XPS data confirmed that the sulfonate group (originating from C8F) can be an effective dopant at the PEDOT material surfaces, and the Cl^- counter ions (from the $FeCl_3$ oxidant) were simultaneously expelled. PPy and PANI synthesized by oxidative coupling polymerizations are doped with sulfate anions rather than Cl^- ions in a preferential manner [23, 24], and the same phenomenon was observed for the PEDOT materials.

The static contact angles of water drops were measured on pressed pellets of the PEDOT materials to study the hydrophilic–hydrophobic balance of PEDOT. The contact angle determined for the PEDOT-C8F particles (104 ± 3°) was higher than that measured for the PEDOT-Cl material (40 ± 2°), which indicates that the hydrophobic surface character of PEDOT-C8F owes to the presence of the C8F dopant. The critical surface tensions of PEDOT-C8F and PEDOT-Cl were determined to be 30 mN/m and 49 mN/m, respectively, by a Zisman plot (Fig. 6).

Conventional four-point probe conductivity measurement studies on the pressed pellet confirmed that the conductivities of the PEDOT-C8F and PEDOT-Cl materials were 15.54 ± 0.02 and 3.82 ± 0.03 S cm^{-1} at 25 °C, respectively (Table 1). The conductivity of PEDOT-C8F was higher than that of PEDOT-Cl, and the C8F sulfonate dopant electrostatically attached to the PEDOT backbone should contribute to the higher conductivity. The PEDOT-C8F particles were both hydrophobic and electrically conductive, which may indicate that the PEDOT-C8F particles possessed dual surfaces from the water-repellent C8F and the electrically conductive PEDOT materials.

To investigate the light-to-heat conversion properties of the PEDOT materials, the temperature changes induced by the NIR laser (808 nm, 200 mW) irradiation were analyzed by thermography. The rapid temperature increases from room temperature to 450 °C and 340 °C were measured by the NIR laser irradiation of the bulk PEDOT-C8F and PEDOT-Cl pressed pellets, respectively (the distance between a laser pointer head and the pellet was 3 cm) (Fig. 7). At these temperatures, the PEDOT materials should start to decompose (see TGA results). Compared to PEDOT-Cl, PEDOT-C8F demonstrated a greater light-to-heat conversion. The photothermal ability of the conjugated

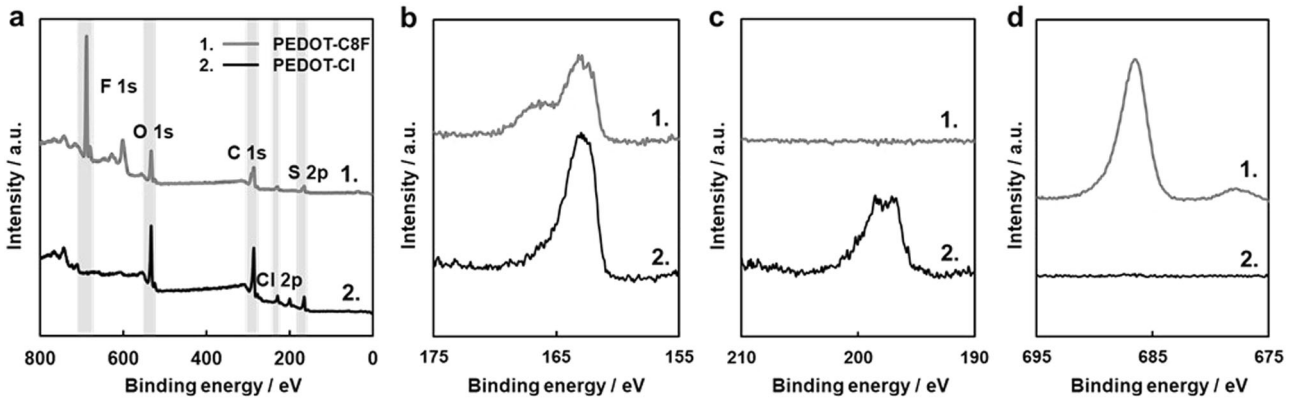

Fig. 5 **a** XPS survey spectra of PEDOT materials: 1) PEDOT-C8F; 2) PEDOT-Cl. **b–d** XPS high resolution spectra of (**b**) S2p, (**c**) Cl2p and (**d**) F1s

Table 2 Surface atomic compositions of PEDOT-C8F and PEDOT-Cl materials as determined by X-ray photoelectron spectroscopy

	Atom %				
	C	S	O	Cl	F
PEDOT-C8F	46.46	16.45	5.48	~0	31.61
PEDOT-Cl	64.47	23.55	8.17	3.8	–

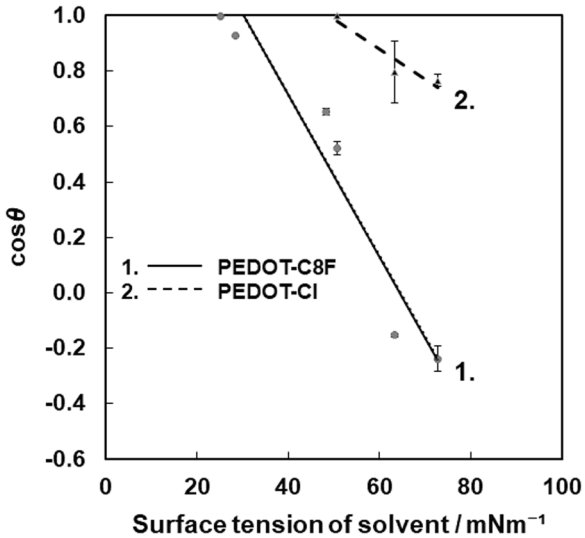

Fig. 6 Zisman plots for 1) PEDOT-C8F and 2) PEDOT-Cl materials. The critical surface tensions (γ_c) were 30 mNm^{-1} and 49 mNm^{-1} for PEDOT-C8F and PEDOT-Cl materials, respectively

polymers is related to the electrical conductivity [33], although the reason remains unclear; the higher the conductivity was, the higher the temperature measured during the NIR laser irradiation. From the results shown above, it has been confirmed that the PEDOT-C8F particles efficiently convert NIR light into heat.

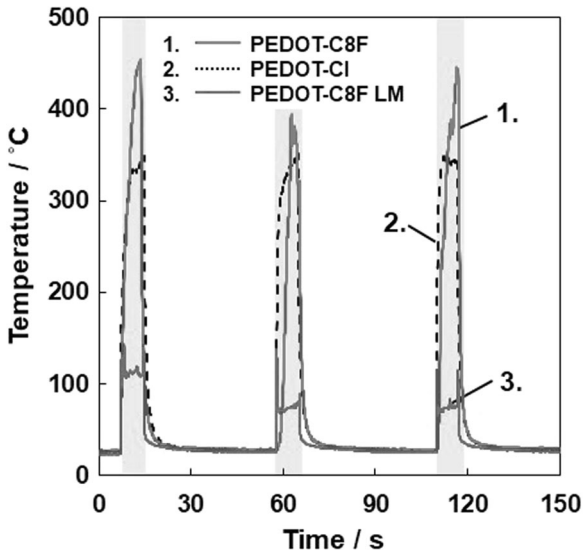

Fig. 7 Surface temperature profiles of 1) PEDOT-C8F, 2) PEDOT-Cl and 3) PEDOT-C8F particle-stabilized LM obtained by thermography. The shaded areas are irradiation periods with an NIR laser

NIR laser-induced movement of PEDOT-stabilized LMs

Individual LMs could be fabricated by rolling a 15 μL (3.0 mm diameter) water droplet over the dried PEDOT-C8F particles (Fig. 8a inset). The water droplet was immediately covered by the dried particles and was prevented from wetting the substrates. The water/PEDOT-C8F weight ratio was gravimetrically determined to be 100/1.1 ± 0.4. These LMs were stable enough to be placed on a planar air–water interface for at least one-week in a closed system (with a glass lid). A LM could also be fabricated using glycerol as the inner liquid. On the other hand, PEDOT-Cl was so hydrophilic that the water and glycerol droplets were absorbed by the powder.

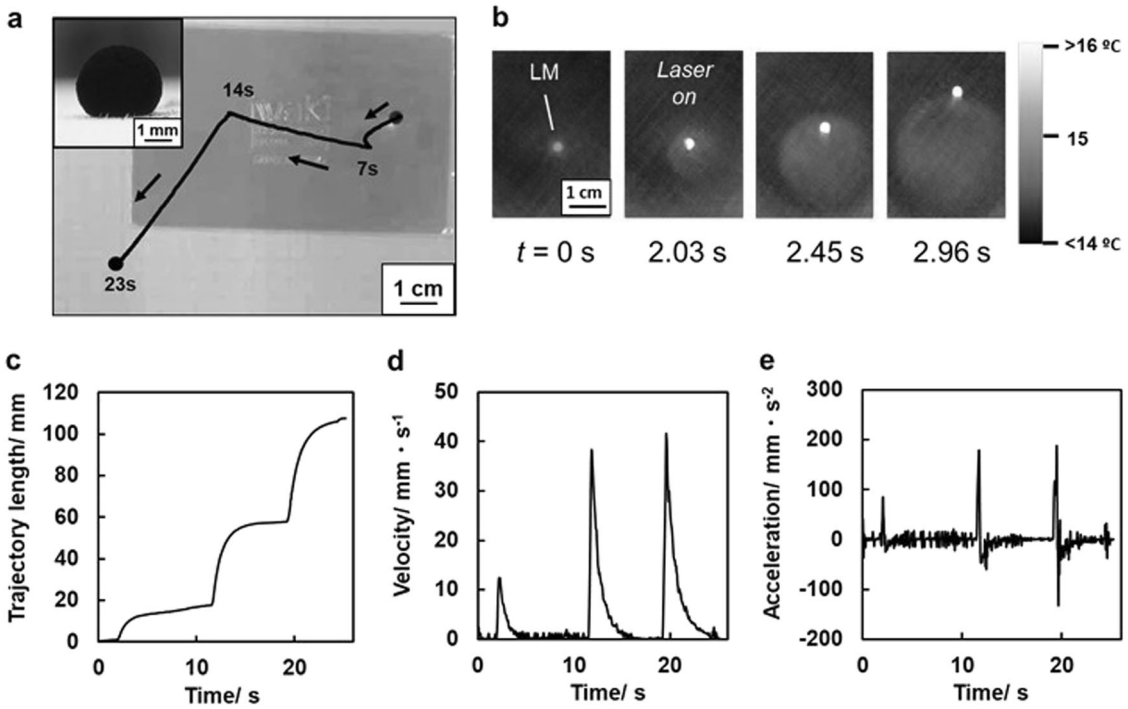

Fig. 8 **a** NIR-driven movement of a PEDOT-C8F particle-stabilized LM on air–water interface. An inset shows the LM placed on plastic substrate. **b** Snapshots of the movement of the PEDOT-C8F particle-stabilized LM observed by thermography. **c**-**e** Profiles of the movement of the PEDOT-C8F particle-stabilized LM: **(c)** pathlength, **(d)** velocity and **(e)** acceleration

The remote control of the movement of small objects has gained increasing interest [34–39] in the fields of science and technology, specifically in material delivery and microfluidic research areas. LMs are expected to be useful materials because they can encapsulate and deliver functional materials (for example, solid particle stabilizers as well as inner liquids) and release them on-demand and at suitable times in response to external stimuli [9]. Here, the movement of the PEDOT-C8F particle-stabilized LMs by near-infrared light-induced Marangoni flow is demonstrated. The existence of PEDOT-C8F particles on the LM surfaces could introduce a light-to-heat conversion ability to the LM. The NIR irradiation of the LM placed on a glass substrate induced a surface temperature increase from 26 °C to over 80 °C within 1 s, which was confirmed by thermography studies (Fig. 7). The temperature increase was lower than that measured for the bulk PEDOT-C8F materials, which could be due to the thin layer of the PEDOT-C8F particle shell on the LM surface and the escape of heat to the encapsulated water. The maximum temperature was lower than the decomposition temperature of PEDOT-C8F, and the decomposition of PEDOT-C8F was unlikely. Movement of the PEDOT-C8F particle-stabilized LM on the planar air–water interface could be induced on-demand by the NIR laser point irradiation of the LM at an angle of ~45°; the contact line of the LM in the air phase and water phase was manually irradiated with the NIR laser pointer. The LM showed movement on the air–water interface in the same direction as the NIR laser irradiation (Fig. 8a and Supplementary Information Movie 1). The movement of the LM could be induced over 45 times. Sunlight condensed by a magnifying glass could also induce the movement of the LM on the air–water interface (Supplementary Information Movie 2).

Snapshots of the NIR light-induced LM movements obtained by thermography offer useful information on the Marangoni flow-assisted movement of the LMs (Fig. 8b). For the NIR laser irradiation, the temperature at one point on the LM surface increased ($t = 0$ s). Then, the heat generated on the LM surface began transferring to the water surface (snapshot at $t = 2.03$ s), which eventually led to the formation of heat flow (snapshot at $t \geq 2.45$ s). The water surface temperature near the local NIR laser-irradiation point of the LM was ~24.8 °C, which was 10.3 °C higher than that of the bulk water surface (14.5 °C). This temperature gradient indicates the formation of a surface tension gradient of ~1.6 mN/m (73.6-72.0 mN/m [40]) around the LM. This surface tension gradient induced the Marangoni flow and drove the LM movement. The NIR light irradiation time of the LM was shorter than one second, and the generated heat could escape to the bulk water, as well as to the encapsulated water and air phase. Under these conditions, the surface temperature of the LM was <70 °C with a maximum temperature of 65 °C.

The LM movement was traced and analyzed (see the Supplementary Information Movie 1 and Fig. 8a, where the black arrows show the movement directions). It is possible to control the movement direction of the LM on the water surface simply by changing the NIR laser irradiation direction, and the average pathlength per NIR laser shot was 35 ± 15 mm ($n = 15$) (Fig. 8c). By the time differentiation of the pathlength and the velocity of the LM movement, the average velocity and positive acceleration were 0.0189 ± 0.0078 m s^{-1} ($n = 15$) and 0.104 ± 0.063 m s^{-2} ($n = 15$), respectively (Fig. 8d, e), which are in the same order of magnitude as those estimated for the movement of the LMs stabilized by the PPy and PANI particles [23, 24]. The deviation in the velocity and acceleration of the LM movement could be due to the difference in the PEDOT-C8F particle shell thickness of the LM and the variation in the NIR laser irradiation positions on the LM surfaces. The decay time of the LM movement was estimated to be 1.18 ± 0.27 s. Using the Newtonian equation of motion, the average force generated by the irradiation was approximately 1.56 μN. Here, the average mass of the LMs was 15.0×10^{-6} kg, and an average positive acceleration was used for the calculation.

LMs are a suitable vehicle for the transport and release of reagents and analytes to/at targeted places. Using the light-responsive LMs developed in this study, it is possible to combine the two concepts: the transport of the LMs based on the near-infrared light-induced Marangoni flow and the external stimulus-responsive release of their inner liquids via disruption. The LM on the planar water surface could be disrupted by the addition of THF near the LM; this may occur as THF is miscible with water and has a lower surface tension (28.5 mN/m [41]) compared to water (73.6 mN/m [40]). This disruption led to the diffusion of the Sunred YM-dyed water (2 wt%) encapsulated by the LM in the water pool (Fig. 9). The planar water surface could be covered by spreading THF, and the THF could wet the PEDOT-C8F particles, creating a gap between the water inside the LM and the water pool underneath the LM. Because of this wetting, the water phases underneath the LM and inside the LM could contact each other, resulting in the disruption of the LM.

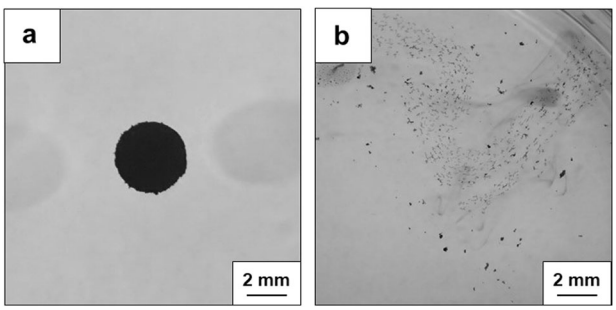

Fig. 9 Digital photographs illustrating stimulus-responsive disruption of the PEDOT-C8F particle-stabilized LM on a planar water surface. Tetrahydrofuran (THF) was added to the water pool (**a**) before and (**b**) after addition of THF. Water encapsulated in the LM (dyed with Sunred YM) diffused into the water pool after the disruption

Conclusions

A facile and versatile synthetic route for the production of perfluoroalkyl dopant-doped hydrophobic PEDOT particles was demonstrated. The XPS studies and contact angle measurements indicated the existence of the perfluoroalkyl dopant on the PEDOT particle surfaces, which provided its water repellent character. The TGA and electrical conductivity measurements confirmed that both the heat stability and the conductivity of the PEDOT-C8F particles were higher in comparison to those of PEDOT-Cl synthesized in the absence of C8F due to the doping with the heptadecafluorooctane sulfonic acid. The PEDOT-C8F particles exhibited light-to-heat conversion properties, and the NIR laser irradiation induced a rapid temperature increase of over 350 °C. The aqueous media-based synthetic method shown in this study requires only commercially available chemicals, and the large-scale production of hydrophobic PEDOT under ambient conditions is feasible. The dried hydrophobic PEDOT-C8F particles can be adsorbed to water droplet surfaces to stabilize LMs. Hydrophobic perfluoroalkyl dopant-doped PEDOT particles can be synthesized by aqueous oxidative coupling polymerization. Furthermore, the LM can move on a planar water surface driven by near-infrared laser-induced Marangoni flow. Considering that the disruption and inner liquid release timing of the LMs can be induced by external stimuli, the LMs shown in this study may have applications in the biomedical and microdevice fields and in light-controlled microfluidics and drug delivery systems.

Acknowledgements We thank Mr. M. Ito for the technical support. This work was supported by a Grant-in-Aid for Scientific Research (B) (JSPS KAKENHI Grant Number JP16H04207) and Scientific Research on Innovative Areas "Engineering Neo-Biomimetics (JSPS KAKENHI Grant Number JP15H01602)" and "New Polymeric Materials Based on Element-Blocks (JSPS KAKENHI Grant Number JP15H00767)". We thank San-Ei Gen F.F.I., Inc. for the kind donation of the Sunred YM dye.

Compliance with ethical standards

Conflict of interest The authors declare that they have no conflict of interest.

References

1. Corradi R, Armes SP. Chemical synthesis of poly(3,4-ethylenedioxythiophene). Synth Met. 1997;84:453–4. https://doi.org/10.1016/S0379-6779(97)80828-4
2. Heywang G, Jonas F. Poly(alkylenedioxythiophene)s - new, very stable conducting polymers. Adv Mater. 1992;4:116–8. https://doi.org/10.1002/adma.19920040213
3. Pei Q, Zuccarello G, Ahlskog M, Inganaes O. Electrochromic and highly stable poly(3,4-ethylenedioxythiophene) switches between opaque blue-black and transparent sky blue. Polymer. 1994;35:1347–51. https://doi.org/10.1016/0032-3861(94)90332-8
4. Kumar A, Reynolds JR. Soluble alkyl-substituted poly(ethylenedioxythiophenes) as electrochromic materials. Macromolecules. 1996;29:7629–30. https://doi.org/10.1021/MA960879W
5. Cheng L, Yang K, Chen Q, Liu Z. Organic stealth nanoparticles for highly effective in vivo near-infrared photothermal therapy of cancer. ACS Nano. 2012;6:5605–13. https://doi.org/10.1021/nn301539m
6. Aussillous P, Quere D. Properties of liquid marbles. Proc R Soc A. 2006;462:973–99. https://doi.org/10.1098/rspa.2005.1581
7. Bormashenko E. Liquid marbles, elastic nonstick droplets: From minireactors to self-propulsion. Langmuir. 2017;33:663–9. https://doi.org/10.1021/acs.langmuir.6b03231
8. McHale G, Newton MI. Liquid marbles: topical context within soft matter and recent progress. Soft Matter. 2015;11:2530–46. https://doi.org/10.1039/C5SM00084J
9. Fujii S, Yusa S, Nakamura Y. Stimuli-responsive liquid marbles: controlling structure, shape, stability, and motion. Adv Funct Mater. 2016;26:7206–23. https://doi.org/10.1002/adfm.201603223
10. Dupin D, Armes SP, Fujii S. Stimulus-responsive liquid marbles. J Am Chem Soc. 2009;131:5386–7. https://doi.org/10.1021/ja901641v
11. Yusa S, Morihara M, Nakai K, Fujii S, Nakamura Y, Maruyama A, et al. Thermo-responsive liquid marbles. Polym J. 2014;46:145–8. https://doi.org/10.1038/pj.2013.84
12. Bormashenko E, Musin A. Revealing of water surface pollution with liquid marbles. Appl Surf Sci. 2009;255:6429–31. https://doi.org/10.1016/j.apsusc.2009.02.027
13. Xue Y, Wang H, Zhao Y, Dai L, Feng L, Wang X, et al. Magnetic liquid marbles: a "precise" miniature reactor. Adv Mater. 2010;22:4814–8. https://doi.org/10.1002/adma.201001898
14. Gao W, Lee HK, Hobley J, Liu T, Phang IY, Ling XY. Graphene liquid marbles as photothermal miniature reactors for reaction kinetics modulation. Angew Chem Int Ed. 2015;54:3993–6. https://doi.org/10.1002/anie.201412103
15. Sheng Y, Sun G, Ngai T, Wu J, Ma G, Ngai T. Silica-based liquid marbles as microreactors for the silver mirror reaction. Angew Chem Int Ed. 2015;54:7012–7. https://doi.org/10.1002/anie.201500010
16. Zang D, Li J, Chen Z, Zhai Z, Geng X, Binks BP. Switchable opening and closing of a liquid marble via ultrasonic levitation. Langmuir. 2015;31:11502–7. https://doi.org/10.1021/acs.langmuir.5b02917
17. Sato E, Yuri M, Nishiyama T, Horibe H, Fujii S, Nakamura Y. Liquid marbles as a micro-reactor for efficient radical alternating copolymerization of diene monomer and oxygen. Chem Commun. 2015;51:17241–4. https://doi.org/10.1039/C5CC07421E
18. Bormashenko E, Pogreb R, Bormashenko Y, Musin A, Stein T. New investigations on ferrofluidics: ferrofluidic marbles and magnetic-field-driven drops on superhydrophobic surfaces. Langmuir. 2008;24:12119–22. https://doi.org/10.1021/la802355y
19. Fujii S, Sawada S, Nakayama S, Kappl M, Ueno K, Shitajima K, et al. Pressure-sensitive adhesive powder. Mater Horiz. 2016;3:47–52. https://doi.org/10.1039/C5MH00203F
20. Dampeirou, C Hydrophobic silica-based powder containing xylitol or trehalose and water for base of cosmetics. 2005: FR2860435A1.
21. Paven M, Mayama H, Sekido T, Butt HJ, Nakamura Y, Fujii S. Light-driven delivery and release of materials using liquid marbles. Adv Funct Mater. 2016;26:3199–206. https://doi.org/10.1002/adfm.201600034
22. Kawashima H, Nakamura Y, Fujii S, Paven M, Butt HJ, Mayama H. Transfer of materials from water to solid surfaces using liquid marbles. ACS Appl Mater Interfaces. 2017;9:33351–9. https://doi.org/10.1021/acsami.7b11375
23. Kawashima H, Mayama H, Nakamura Y, Fujii S. Hydrophobic polypyrroles synthesized by aqueous chemical oxidative polymerization and their use as light-responsive liquid marble stabilizers. Polym Chem. 2017;8:2609–18. https://doi.org/10.1039/C7PY00158D
24. Kawashima H, Okatani R, Mayama H, Nakamura Y, Fujii S. Synthesis of hydrophobic polyanilines as a light-responsive liquid marble stabilizer. Polymer. 2018;148:217–27. https://doi.org/10.1016/j.polymer.2018.06.039
25. Inoue H, Hirai T, Hanochi H, Oyama K, Mayama H, Nakamura Y, et al. Poly(3-hexylthiophene) grains synthesized by solvent-free oxidative coupling polymerization and their use as light-responsive liquid marble stabilizer. Macromolecules. 2019;52:708–17. https://doi.org/10.1021/acs.macromol.8b02426
26. Kavokine N, Anyfantakis M, Morel M, Rudiuk S, Baigl D, Bickel T. Light-driven transport of a liquid marble with and against surface flows. Angew Chem Int Ed. 2016;55:11183–7. https://doi.org/10.1002/anie.201603639
27. Zhao Q, Jamal R, Zhang L, Wang M, Abdiryim T. The structure and properties of PEDOT synthesized by template-free solution method. Nanoscale Res Lett. 2014;9:557 https://doi.org/10.1186/1556-276X-9-557
28. Lin-Vien, D, Colthup, NB, Fateley, WG & Grassetti, JG. The Handbook of Infrared and Raman Characteristics Frequencies of Organic Molecules *Academic Press, Inc*. (1991)
29. Han, CC, Lee, JT, Yang, RW, Chang, H & Han, CH. A new and easy method for making micrometer-sized carbon tubes. *Chem. Commun*. 2087–8 (1998) https://doi.org/10.1039/a805057k
30. Fujii S, Matsuzawa S, Nakamura Y, Ohtaka A, Teratani T, Akamatsu K, et al. Synthesis and characterization of polypyrrole-palladium nanocomposite-coated latex particles and their use as a catalyst for Suzuki coupling reaction in aqueous media. Langmuir. 2010;26:6230–9. https://doi.org/10.1021/la9039545
31. Rozlivkova Z, Trchova M, Exnerova M, Stejskal J. The carbonization of granular polyaniline to produce nitrogen-containing carbon. Synth Met. 2011;161:1122–9. https://doi.org/10.1016/j.synthmet.2011.03.034
32. Moravkova Z, Trchova M, Exnerova M, Stejskal J. The carbonization of thin polyaniline films. Thin Solid Films. 2012;520:6088–94. https://doi.org/10.1016/j.tsf.2012.05.067
33. Wu C-Y, Benatar A. Microwave welding of high density polyethylene using intrinsically conductive polyaniline. Polym Eng Sci. 1997;37:738–43. https://doi.org/10.1002/pen.11717
34. Wang J. Can man-made nanomachines compete with nature biomotors? ACS Nano. 2009;3:4–9. https://doi.org/10.1021/nn800829k
35. Mirkovic T, Zacharia NS, Scholes GD, Ozin GA. Fuel for thought: chemically powered nanomotors out-swim nature's flagellated bacteria. ACS Nano. 2010;4:1782–9. https://doi.org/10.1021/nn100669h
36. Yamamoto D, Shioi A. Self-propelled nano/micromotors with a chemical reaction: Underlying physics and strategies of motion control *KONA Powder and Particle*. Powder Part J. 2015;32:2–22. https://doi.org/10.14356/kona.2015005

37. Wang H, Pumera M. Fabrication of micro/nanoscale motors. Chem Rev. 2015;115:8704–35. https://doi.org/10.1021/acs.chemrev.5b00047
38. Sanchez S, Soler L, Katuri J. Chemically powered micro- and nanomotors. Angew Chem Int Ed. 2015;54:1414–44. https://doi.org/10.1002/anie.201406096
39. Xu L, Mou F, Gong H, Luo M, Guan J. Light-driven micro/nanomotors: from fundamentals to applications. Chem Soc Rev. 2017;46:6905–26. https://doi.org/10.1039/C7CS00516D
40. Vargaftik NB, Volkov BN, Voljak LD. International tables of the surface tension of water. J Phys Chem Ref Data. 1983;12:817 https://doi.org/10.1063/1.555688
41. Ramkumar DHS, Kudchadker AP. Mixture properties of the water + .gamma.-butyrolactone + tetrahydrofuran system. Part 2. Viscosities and surface tensions of.gamma.-butyrolactone + water at 303.15-343.15 K and.gamma.-butyrolactone + tetrahydrofuran at 278.15-298.15 K. J Chem Eng Data. 1989;34:463–5. https://doi.org/10.1021/je00058a027